Original

Porous ceramic supported TiO2 nanoparticles: Enhanced photocatalytic activity for Rhodamine B degradation

Allan Ramone de Araujo Scharnberg [a,b,*], Adrison Carvalho de Loreto [b],
Tiago Bender Wermuth [a], Annelise Kopp Alves [a], Sabrina Arcaro [c],
Pâmela Andréa Mantey dos Santos [b], Adriane de Assis Lawisch Rodriguez [b]

[a] Laboratory of Ceramic Materials, Department of Materials, Federal University of Rio Grande do Sul – UFRGS, Osvaldo Aranha 99, Porto Alegre, RS 90035-190, Brazil
[b] University of Santa Cruz do Sul, Independencia Av, 2293, Santa Cruz do Sul, RS 96815-900, Brazil
[c] Graduate Program in Materials Science and Engineering (PPGCEM), Laboratory of Technical Ceramics (CerTec), Universidade do Extremo Sul Catarinense (UNESC), Av. Universitária 1105, P.O. Box 3167, 88806-000 Criciúma, SC, Brazil

ARTICLE INFO

ABSTRACT

Photocatalytic processes are an efficient and important technique to mineralize organic contaminants in aqueous effluents. However, it is paramount that there is a way to recover the catalyst after degradation. Based on this problem, this research seeks to evaluate the photocatalytic properties of TiO$_2$ under porous ceramics support for the degradation of Rhodamine B (RhB). TiO$_2$ was synthesized by sol-gel, dried at 100 °C and calcined at 400 °C. The morphological, optical and structural proprieties of the particles were characterized. The XRD patterns of samples calcined at 400 °C showed only the anatase phase, confirmed by Raman. Not heat-treated xerogel was amorphous. The agglomerates are composed of fine particles, in the nanometric scale of 15 nm. The bandgap of the powder is 3.21 eV, and the surface area is 60.1 m^2 g^{-1}. To evaluate its photocatalytic activity, the anatase TiO$_2$ was supported in a porous ceramic substrate by a dip-coating process. The heterogeneous photocatalysis showed excellent results, with the degradation of up to 83% of RhB. It was possible obtained with successful an efficient technique for the treatment of wastewater with Anatase nanoparticles supported in the ceramic support obtained from of reuse of the residues.

© 2019 SECV. Published by Elsevier España, S.L.U. This is an open access article under the CC BY-NC-ND license (http://creativecommons.org/licenses/by-nc-nd/4.0/).

Nanopartículas de TiO$_2$ suportadas en cerámica porosa: actividad fotocatalítica mejorada para el tratamiento de la rodamina B

RESUMEN

Palabras clave:
Fotocatálisis heterogénea
Nanopartículas de TiO$_2$
Rodamina B
Cerámica porosa

Los procesos fotocatalíticos son técnicas eficientes para la mineralización de contaminantes orgánicos en efluentes acuosos. Sin embargo, es fundamental que haya una forma de recuperar el catalizador después de la degradación. En base a este problema, esta investigación busca evaluar las propiedades fotocatalíticas del dióxido de titanio (TiO$_2$) bajo el soporte de cerámica porosa para la degradación de la rodamina B (RhB). El TiO$_2$ se sintetizó mediante sol-gel, se secó a 100 °C y se calcinó a 400 °C. Se caracterizaron las propiedades morfológicas, ópticas y estructurales de las partículas. Los patrones DRX de las muestras calcinadas a 400 °C mostraron solo la fase anatasa, confirmada por Raman. El xerogel no tratado térmicamente era amorfo. Los aglomerados están compuestos de partículas finas, en la escala de 15 nm. El intervalo de banda es de 3,21 eV, y el área de superficie es de 60,1 m^2.g^{-1}. Para evaluar la actividad fotocatalítica, se recubrió un sustrato cerámico poroso mediante el proceso de recubrimiento por inmersión. La fotocatálisis heterogénea mostró excelentes resultados, con la degradación de hasta el 83% de la RhB. Fue posible obtener con éxito una técnica eficiente para el tratamiento de aguas residuales con nanopartículas de anatasa soportadas en el soporte cerámico obtenido de la reutilización de los residuos.

Introduction

Nowadays the management of wastes generated by industrial operations represents a challenge for a sustainable world. The management of wastes may comprise steps of collection, transportation, treatment, recycling, and landfill disposal after reducing the volume. An issue of concern from the environmental perspective is the water pollution caused by organic dyes. Wastewater containing dyes represents a serious environmental problem because of the high toxicity and possible accumulation of these dyes in the environment due to their carcinogenic and mutagenic effect [1].

Furthermore, dyes in textile mill effluents, in agates dyeing industries and dye industry of paper, may induce antagonistic and synergistic toxicological effects in aquatic life and human health. Rhodamine is one of the most common dyes used in this process [2,3]. The non-biodegradable nature of organic dyes and their high color intensity can also reduce aquatic diversity by blocking the passage of sunlight through the water, especially in the process of photosynthesis and oxygenation of the water spring that receives this effluents [2,4,5]. Besides, these organic dyes are commonly employed as a model molecule in degradation tests [6,7].

Advanced oxidation processes (AOPs) have been mainly the most engaged approach for the reduction of dyes in environmental matrices [5]. The AOPs are based on the *in situ* generations of strong oxidants, mainly hydroxyl radicals (OH$_o$) for the oxidation of organic compounds, capable of mineralizing organic matter to non-toxic forms such as CO$_2$ and H$_2$O [8]. Hydroxyl radicals formation can occur in some ways, especially by combining UV radiation with ozone (O$_3$/UV), hydrogen peroxide (H$_2$O$_2$/UV), fenton and photo-fenton reactions (H$_2$O$_2$/Fe/UV), ultrasound, electrochemical oxidation (individual anodes), and heterogeneous photocatalysis [9].

The heterogeneous photocatalysis technique has been widely studied as a method of destruction of organic and inorganic pollutants [8,10–14]. The process involves redox reactions induced by radiation on the surface of mineral semiconductors used as catalysts [11].

One of the most utilized photocatalysts is the titanium dioxide (TiO$_2$), it is a polymorphous material and may present in the rutile, anatase and brookite phases [15]. The anatase phase, most commonly used, shows tetragonal crystalline structure, and is formed at low temperatures, around 450 °C [16]. The excellent performance of TiO$_2$ in heterogeneous photocatalysis processes is due it is insoluble in water, non-toxic, photostable and chemically stable over a wide range of pH [17]. Various routes can synthesize TiO$_2$: sol-gel; condensation to inert gas; plasma evaporation; hydrothermal microwave-assisted; ultrasonic spray pyrolysis; hydrothermal techniques; and chemical vapor deposition, among others [8,18,19,17,20]. The sol-gel method is widely used in the production of oxide nanoparticles, given its low-cost and environmentally friendly character, coupled to the fact that it allows for the fine-tuning of several synthesis parameters [21].

For an effective heterogeneous photocatalysis, the photocatalysts can be used suspended in the solution or supported on some substrate. Reactors with suspended particles are more common for research in the laboratory [22]. The main advantage of these reactors is the high specific surface area of suspended catalyst particles, which contributes to the higher degradation rate of pollutants. However, for practical applications in large-scale, reactors with immobile TiO$_2$ are preferred, because in this way the operation can be carried out continuously, and separation of catalyst particles at the end of the process is not required. Also, the supported photocatalytic carriers can be reused for several cycles, since in systems with suspended catalysts the particles can hinder the passage of

light into the solution or further sediment, thus not being available for the process [23].

Like suspended photocatalysts, immobilized photocatalysts also have some downsides. In this case, the available reaction surface is reduced decreasing the degradation rate [24]. Because of that, the cycle of photocatalytic treatment has to be prolonged, lowering the daily capacity of treatment. In this respect, porous supports, especially clay-based, are very interesting because they are highly available in the earth's crust, cheap, and show mechanical, thermal and chemical stability [25]. Clays provide TiO$_2$ with the high surface area, porosity, high number of surface active sites, improving the efficiency of the photocatalysis process [12–14].

In this context, the present work seeks to evaluate the potential of discoloration of Rhodamine B, in the process of heterogeneous photocatalysis using nanostructured titanium dioxide supported on porous ceramic material. For this study, the TiO$_2$ was produced by sol-gel synthesis, and characterized by structural, morphological and optical properties. Then, the TiO$_2$ was deposited by dip coating on the porous ceramic support and has shown promising results in the photocatalytic process.

Experimental

The synthesis of nanostructured TiO$_2$ was performed by the sol-gel method [21]. The reagents were isopropyl alcohol 70% (Sigma Aldrich/Germany), titanium tetraisopropoxide (TIPT IV) 97% (Sigma Aldrich/Germany) and ultra-pure type 2 water (MilliQ, 18 MΩ cm) in 3.27;1.62;1 relation (vol/vol). Initially, the isopropyl alcohol was mixed with TIPT IV. The mixture was homogenized on a heating plate (BioMixer, 78HW-1) at 60 °C for 1 h, after which water was added to the system. After that, the temperature was raised to 100 °C, and the mixture was stirred for another 2 h until a gel was obtained. Finally, the TiO$_2$ was dried (Marte, MB 150/6) at 100 °C for 1 h until the formation of a xerogel and heat-treated in a muffle furnace (Jung, 9613) at 2 °C min^{-1} and a plateau of 2 h at 400 °C. The crystallinity of the synthesized TiO$_2$ samples was determined by X-Ray Diffraction (XRD) using a Philips X'Pert MDP diffractometer equipped with a Cu Kα radiation source (λ = 1.5418 Å), 40 kV, 40 mA, step of 0.02°/s, dwell time of 2 s per step and 2θ between 10 and 90° 2θ angle range. The surface area was determined using Brunauer–Emmett–Teller (BET) analysis, with the support of an Autosorb Quantachrome Instrument Nova 1000 device. The diffuse reflectance was done with the Agilent Cary 5000 UV–Vis–NIR universal measurement spectrophotometer in wavelength between 190 nm and 1200 nm. The Scanning Electron Microscopy (SEM) technique was used for the morphological characterization of the powder and ceramics substrate. The analysis was carried out in a Carl Zeiss, model EVO MA10 at 10 kV. The Raman experiments were carried out on Renishaw inVia™ Spectrometer System for Raman spectral analysis, using a 532 nm laser.

The TiO$_2$ synthesized was supported in a porous ceramic (60 × 20 × 5 mm) produced by the study group previously [26]. This porous ceramic is composed of 60% red clay and 40% of residues (20% glass powder, and 20% yerba mate), heat-treated at 1100 °C. Several formulations were studied; tests

of linear retraction, water absorption, apparent porosity, and mechanical strength were performed. This configuration was select due it presents values of residue aggregation of 40% and yet exhibits satisfactory properties when compared to the material without the addition of residues, like apparent porosity (26.19 ± 0.25%) and water absorption (17.69 ± 0.43%). Furthermore, good mechanical strength was obtained (7.93 ± 0.26 MPa) [26].

Two suspensions were obtained from catalyst and the deposition was evaluated: Suspension (a) with 5 g of TiO$_2$ in 100 mL of ultra-pure water (Milli-Q) [27], and suspension (b): 5 g de TiO$_2$ and 10 mL of ultra-pure water (Milli-Q) in 90 mL of alcohol [28]. The suspensions were homogenized on a magnetic stirrer (BioMixer/78HW-1) for 24 h until complete dispersion of the catalyst in the solution. After homogenization, the catalyst was deposited on ceramic material by a home-made *dip-coating* technique. Fifty immersions were performed in each ceramic substrate by 1 min. To obtain the exact value of the catalyst involved in the reaction, only one side of the substrate received the material; the others were isolated.

After impregnation, the porous ceramics were dried (Marte, MB150/6) at 100 °C for 60 min and then thermally treated in a muffle (Jung, 9613), with a heating rate of 2 °C min^{-1} at 400 °C in 60 min. The amount of photocatalyst supported in the porous ceramic was obtained by the difference in their mass before and after the impregnation process.

For each analysis, 500 mL of Rhodamine B solution was used to simulate the effluent. A magnetic stirrer (BioMixer/78HW-1) was used, to maintain stirring during the tests. Fig. 1 shows the diagram of the reactor used. A low irradiation source was used (an 11W UV lamp/Osram), isolated from the solution by a quartz tube. Due to its low power, it does not change the temperature of the solution, and then the tests were performed at room temperature (20 °C). Four substrates were placed per test, totaling 0.28 g of TiO$_2$, and application factor of 560 mg of TiO$_2$ per liter of effluent, affixed in a circular metal holder, with the catalyst containing face to the lamp.

Simulating a real effluent, a concentration of 5 mg L^{-1} of Rhodamine B in deionized water was used. To relate the
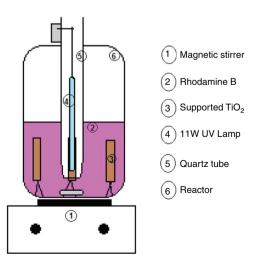

Fig. 1 – Reactor utilized during the heterogeneous photocatalysis tests.

Table 1 – Configurations proposed to evaluate the degradation of Rhodamine B.

Config.	Description	Function
A	UV lamp + ceramics with TiO$_2$;	Heterogeneous photocatalysis
B	UV lamp + ceramics without TiO$_2$;	Adsorption and photolysis
C	UV lamp	Photolysis
D	Ceramics with TiO$_2$;	Adsorption

level of Rhodamine B, during the photocatalysis tests with its absorbance reading, a calibration curve of Rhodamine B was elaborated, where the results of absorbance were analyzed in a spectrophotometer (V-1100) with wavelength (λ_{max}) for Rhodamine B at 550 nm [29]. The calibration curve for Rhodamine B presented linear regression equation $y = 0.0044x - 0.3406$ and a coefficient of determination (R^2) of 0.9981, showing good linearity.

The heterogeneous photocatalysis degradation tests were performed for 120 min with aliquot withdrawals every 10 min for absorbance analysis in the first 60 min. After this, an aliquot was withdrawals at 90 and 120 min for each assay. It was proposed four configurations to evaluate the influence of heterogeneous photocatalysis, photolysis, and adsorption on effluent degradation, according to Table 1:

The kinetics of photocatalysis reactions best fit the Langmuir–Hinshelwood Model (Eq. (1)), with a pseudo-first-order degradation rate. In addition to the kinetic constant, it is possible to calculate the half-life time (Eq. (2)), a parameter that expresses the time required for the concentration of the solution in question to decrease to half of its initial value [30].

$$k_{ap} \cdot t = \ln \left(\frac{C_0}{C} \right) \tag{1}$$

$$t_{1/2} = \ln \left(\frac{2}{k_{ap}} \right) \tag{2}$$

where k_{ap} is the apparent kinetic constant of the reaction (min^{-1}); t is the elapsed time (min); C_0 is the initial concentration; C is the concentration at time t; $t_{1/2}$ is the half-life time (min).

Results and discussion

TiO$_2$ characterizations

To evaluate the structure of obtained materials, XRD analysis was performed. Fig. 2 displays the diffractograms of the xerogel (Not heat treated) and the samples thermally treated at 400 °C (Heat treated). As expected, the xerogel has demonstrated an amorphous structure, which can be accomplished from the broad characteristic diffraction peak between 2$\theta \sim$ 20° and 30°. On the other hand, all the diffraction peaks of the sample heat-treated at 400 °C are indexed to be representative of the pure anatase phase (JCPDS 01-071-1166) with tetragonal structure indicating the successful preparation of the TiO$_2$ *via* the proposed synthesis pathways. Furthermore, this diffractogram presents a marked broadening of the reflections,
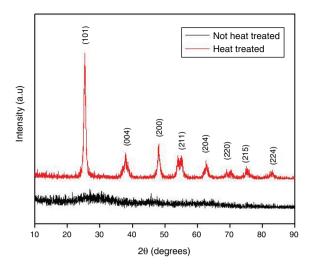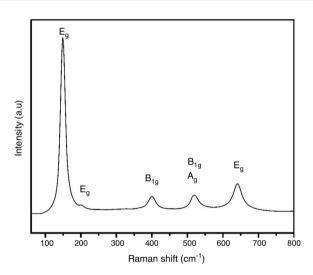

Fig. 2 – X-ray diffraction plot for TiO$_2$.

Fig. 3 – Raman spectrum of TiO$_2$ anatase synthesized by sol-gel method.

which means crystallite sizes on a nanometric scale. The application of the Scherrer equation to the experimental curves yields lower limits of average crystallite size of 15 nm thereby confirming the formation of nanostructured TiO$_2$ with structure anatase.

The crystal structure of thermally treated at 400 °C sample can be confirmed by Raman spectroscopy studies and it is shown in Fig. 3. Anatase has six Raman active modes: Eg(1) (149 cm^{-1}), Eg(2) (199 cm^{-1}), B1 g(1) (399 cm^{-1}), A1 g/B1 g(2) (overlapped at 519 cm^{-1}), and Eg(3) (641 cm^{-1}) [31]. The presence of the Eg(2) peak, which is usually very hard to detect, evidences the high degree of crystallinity of the samples.

To evaluate the obtained morphologies, SEM studies were performed. In Fig. 4 it is observed the formation of agglomerates in both the TiO$_2$ xerogel and the anatase (sample thermally treated TiO$_2$ sample at 400 °C). The agglomerates are composed of fine particles, in the nanometric scale in the case of the sample heat-treated at 400 °C. The nanoparticles are highly reactive, which promotes the formation of
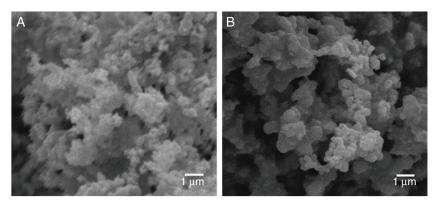
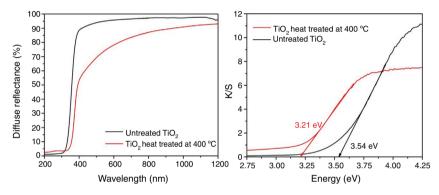Fig. 4 – Scanning electron microscope (SEM) image of (A) anatase and (B) amorphous TiO$_2$.

Fig. 5 – UV/vis spectrum of TiO$_2$ showing diffuse reflectance (DRS) from 200 to 1200 nm and Kubelka–Munk plot showing indirect band gap value of 3.54 eV for untreated TiO$_2$ and 3.21 eV for anatase.

agglomerates. The surface area of the particles has been evaluated by BET and is 60.106 m^2 g^{-1}, which can be considered very high if compared with anatase prepared by the sol-gel route [18].

The UV–Vis diffuse reflectance spectra of the TiO$_2$ powders synthesized heat-treated at 400 °C, and untreated TiO$_2$ (xerogel) are shown in Fig. 5. An evident semiconducting behavior can be inferred from the optical assays in both samples. To estimate the optical bandgap of the different samples, the Kubelka–Munk method was applied to the reflectance curves. The estimated band gap value is 3.21 eV. It worth noting which it is typical of quantum effects in nanocrystallites, and it has been found that the bandgap shifts to a lower wavelength (or higher energy) with decreasing crystallite size [32]. Moreover, the usual value of E_g for the anatase phase synthesized by sol-gel is 3.2 eV [21,33]. Amorphous TiO$_2$ usually present E_g values greater than crystalline forms, mainly due to the structural defects [34]. The xerogel dried at 100 °C show a bandgap of 3.54 eV, which is also a semiconductor but can absorb less light than the anatase phase (crystalline).

Deposition of TiO$_2$ in the ceramic substrate

After a complete characterization of the TiO$_2$ synthesized by sol-gel, TiO$_2$ was supported in the porous ceramic. The supports were weighed before and after the impregnation process and the difference, after the dry process, we consider

as the supported amount. The weight of TiO$_2$ impregnated in the porous ceramic, from the suspension containing only water was 50.5 ± 4 mg. On the other hand, from the suspension containing alcohol as dispersing media, it was possible to impregnate 70.2 ± 1 mg. One perceives that the alcohol suspension proved to be more efficient as it was possible to impregnate a more significant amount of catalyst in the ceramics substrate. This phenomenon indicates that the nanoparticles were more dispersed in alcohol remaining in suspension and having a viscosity more suitable for deposition, giving greater homogeneity to the deposited layer [28]. The alcohol addiction changed the pH of the system from 6.8 to 5.1. It is reported that the addition of alcohol to the suspension containing TiO$_2$ and H$_2$O may affect the potential zeta values of the particles and increase the viscosity of the suspension [35]. In this case, this situation is beneficial as a slightly higher viscosity can improve particle adhesion to the substrate surface. To evaluate the deposition of TiO$_2$ nanoparticles from the suspension containing alcohol as a dispersing agent, the samples were assessed by SEM. Fig. 6 shows the SEM micrograph of the porous ceramic support before TiO$_2$ impregnation and porous ceramic supported TiO$_2$ nanoparticles. The micrographs show the porous surface of the substrate without deposition of TiO$_2$ and subsequent deposition. It is observed a good homogeneity of the photocatalyst on the support without excess agglomeration of the particles.

Table 2 – Results of heterogeneous photocatalysis applied to Rhodamine B degradation.

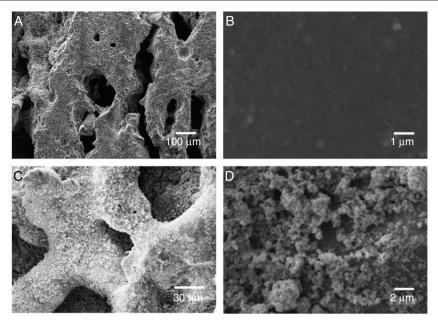| Conf.	Description	C/C_0	k_{ap} (min^{-1})	Half-life time ($t_{1/2}$) (min)	R^2
A	UV/CP/TiO$_2$	0.47	6.27×10^{-3}	110.55	0.9865
B	UV/CP	0.86	1.30×10^{-3}	533.19	0.9179
C	UV	0.80	1.81×10^{-3}	382.95	0.9624
D	CP/TiO$_2$	1.00	0.06×10^{-3}	∼	0.1039
L-T*	UV/CP/TiO$_2$	0.17	5.77×10^{-3}	120.12	0.9783

Fig. 6 – Scanning electron microscope (SEM) image of the porous ceramics substrate before (A e B) and after (C e D) TiO$_2$ deposition in different magnifications.

Heterogeneous photocatalysis

To evaluate the photocatalytic properties of the catalyst, photocatalysis tests of RhB dye were performed. Table 2 shows the results for the remaining concentration of Rhodamine B (C/C_0), reaction kinetics k_{ap} (min^{-1}), half-life time (min) and determination coefficient (R^2) obtained in the four configurations tested for degradation of Rhodamine B in 120 min. The L-T* configuration refers to the long-term performed with the A configuration by 5 h.

The best results were obtained with heterogeneous photocatalysis (A), with the degradation of 53% in 120 min of the test, a half-life time of 110 min. The purpose of the catalyst without UV radiation (D) did not change the solution after 120 min, showing that there is no adsorption on the supporting material. The contribution of the direct adsorption of Rhodamine B to TiO$_2$ (CP/TiO$_2$) is negligible. This behavior also suggests that the surface of the support is very well coated, since there was no reduction in the color of the solution, as in curve B where the substrate, without TiO$_2$, was exposed to UV light where a
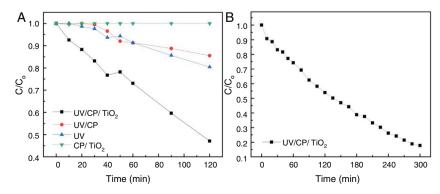

Fig. 7 – Results obtained in the four configurations tested for 2 h (A) and the L-T* configuration test for 5 h (B) demonstrating the gradual degradation of Rhodamine B.

Table 3 – Comparison of Rhodamine B degradation in the literature.

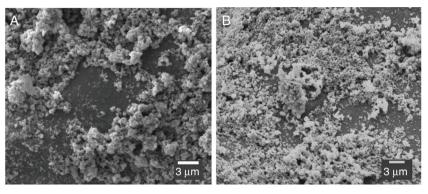| Reference	Catalyst	Conditions	Efficiency (%)
Yin et al. [10]	500 mg L^{-1}, P-25, suspended	50 mg L^{-1}, 400 W Xe – 420 nm, 2 h	80
Wermuth et al. [37]	1490 mg L^{-1}, Sol-gel anatase Polymer anchored	20 mg L^{-1}, 15 W, 3 h	99
Knak de Almeida et al. [18]	500 mg L^{-1} Sol-gel anatase suspended	5 mg L^{-1}, 32 W, 8 h	71
		5 mg L^{-1}, 48 W, 8 h	89
	2000 mg L^{-1} Sol-gel anatase suspended	5 mg L^{-1}, 32 W, 8 h	91
		5 mg L^{-1}, 48 W, 8 h	96
Luttrell et al. [12,36]	160 mg L^{-1}, suspended	10^{-4} M, 100 W, 6 h	80
Mishra et al. [12,38]	500 mg L^{-1}, suspended	10 mg L^{-1}, 800 W, 6 h	88
Present study	560 mg L^{-1} TiO$_2$/porous ceramic	5 mg L^{-1}, 11 W, 5 h	83

Fig. 8 – SEM micrographs of catalyst adhered to the ceramic substrate before (A) and after use in heterogeneous photocatalysis (B).

decrease of 15% was observed, similar as the photolysis (UV) behavior. Photolysis (C – when only UV radiation is used) presented results about 20% of degradation, proving the efficiency of the use of heterogeneous photocatalysis, associating the use of UV light with TiO$_2$. The configuration without the use of a catalyst (UV/CP) had a reduction of 14%, due to the use of UV light, since there is no adsorption of the material. Due to the linearity of the end of the test with the configuration of heterogeneous photocatalysis (A = UV/CP/TIO$_2$), this was repeated, seeking to evaluate its degradation capacity for a longer time, until there was no variation of the concentration, which was reached with 300 min of the test (L-T* of Table 2). The results are shown in Fig. 7.

The degradation efficiency of Rhodamine B by TiO$_2$ supported on porous ceramics by heterogeneous photocatalysis was also compared to the literature (Table 3). This demonstrated that the synthesized TiO$_2$ supported at porous ceramic is capable of achieving high removal efficiency of Rhodamine B under a low lamp power, just 11 W, thus saving energy. It is important to note the application of only 560 mg L^{-1} of catalyst. The same table demonstrates some results of similar experiments using suspended catalysts [10,36]. It is possible to note similar degradation results, yet in immobilization design, it is possible to recover the catalyst easily.

Configuration A, which represents the heterogeneous photocatalysis, presented a constant kinetic k_{ap} of 6.27×10^{-3} or 0.00627 min^{-1} (Fig. 9). This result is in good agreement with the literature. However, the main difference is that the Rhodamine B dye, the focus of this study, is considered to be more
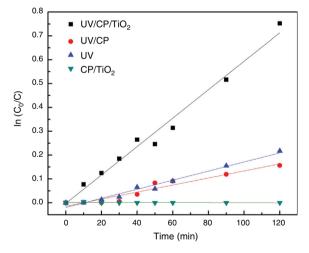

Fig. 9 – The reaction kinetics for all dye degradation tests.

challenging to degrade due to its molecular structure with more complex carbon chains compared to methylene blue. Wermuth et al., 2013, reached a k_{ap} of 28.6×10^{-3} min^{-1}, using different parameters, such as a 15 W lamp and a higher concentration of TiO$_2$ and Rhodamine B, factors that may have influenced kinetics.

Microstructural images (SEM) of the clay substrates coated before and after use in the photocatalysis process are shown in Fig. 8. The images show that most of the catalyst remained adhered to the ceramics after the degradation of the

Rhodamine B effluent. This phenomenon demonstrates that the use of the supported TiO_2 is very efficient since the photoactive material can be easily recovered [24]. Also, only a minor quantity of the catalyst is lost in the reactor, along with the effluent. Another possibility of testing is using the continuous flux regime. In this way, it is possible to treat a more significant amount of effluent in this method than in the batch flow with the same catalyst.

Conclusions

It was possible to synthesize titanium dioxide (TiO_2) nanostructured by the sol-gel method. The DRX and Raman characterizations showed the oblation of anatase phase and crystallite size of 15 nm. Also, the SEM images illustrated that was performed a deposition a uniform layer of 70 mg of the catalyst in the ceramic material, using the dip-coating method, and that after the usage, a major part of the catalyst stays at ceramics, it makes possible to recover it or even executes a continuous flow reactor. Higher deposition efficiency was confirmed using alcohol in the solution media compared to only water. The application of the catalyst in the heterogeneous photocatalysis showed excellent results, with the removal of up to 83% of the coloration Rhodamine B, mainly due to the structure of the synthesized catalyst and the anchorage process. It brings an efficient technique for the treatment of this problematic dye and a method of reuse of the residues employed in the manufacture of the ceramic support.

Acknowledgments

REFERENCES

[1] M. Tasbihi, I. Călin, A. Šuligoj, M. Fanetti, U. Lavrenčič Štangar, Photocatalytic degradation of gaseous toluene by using TiO_2 nanoparticles immobilized on fiberglass cloth, J Photochem Photobiol A: Chem 336 (2017) 89–97, http://dx.doi.org/10.1016/j.jphotochem.2016.12.025.

[2] E. Carissimi, T.M. Pizzolato, A. Zoch, C. Mistura, E.L. Machado, I.A.H. Schneider, Treatment of dye bearing effluents from Brazilian agate industry, Dev Miner Process 13 (2000) 9Cb–C12b, http://dx.doi.org/10.1016/S0167-4528(00)80100-3.

[3] A.L.D. da Rosa, E. Carissimi, G.L. Dotto, H. Sander, L.A. Feris, Biosorption of rhodamine B dye from dying stones effluents using the green microalgae Chlorella pyrenoidosa, J Clean Prod 198 (2018) 1302–1310, http://dx.doi.org/10.1016/J.JCLEPRO.201807128.

[4] A.L. Barros, T.M. Pizzolato, E. Carissimi, I.A.H. Schneider, Decolorizing dye wastewater from the agate industry with Fenton oxidation process, Miner Eng 19 (2006) 87–90, http://dx.doi.org/10.1016/J.MINENG.200504004.

[5] T. Pizzolato, E. Carissimi, E. Machado, I.A. Schneider, Colour removal with NaClO of dye wastewater from an agate-processing plant in Rio Grande do Sul, Brazil, Int J Miner Process 65 (2002) 203–211, http://dx.doi.org/10.1016/S0301-7516(01)00082-5.

[6] X. Yin, X. Li, W. Gu, F. Wang, Y. Zou, S. Sun, Z. Fu, Y. Lu, Enhanced photocatalytic activities of g-C_3N_4 via hybridization with a Bi–Fe–Nb-containing ferroelectric pyrochlore, 2017, http://dx.doi.org/10.1021/acsami.7b04587.

[7] P. Wilhelm, D. Stephan, Photodegradation of rhodamine B in aqueous solution via SiO_2@TiO_2 nano-spheres, J Photochem Photobiol A: Chem 185 (2007) 19–25, http://dx.doi.org/10.1016/J.JPHOTOCHEM.200605003.

[8] X. Qiao, S. Biswas, W. Wu, F. Zhu, C.-H. Tung, Y. Wang, Selective endoperoxide formation by heterogeneous TiO_2 photocatalysis with dioxygen, Tetrahedron 74 (2018) 2421–2427, http://dx.doi.org/10.1016/J.TET.201803040.

[9] D.B. Miklos, C. Remy, M. Jekel, K.G. Linden, J.E. Drewes, U. Hübner, Evaluation of advanced oxidation processes for water and wastewater treatment – a critical review, Water Res 139 (2018) 118–131, http://dx.doi.org/10.1016/J.WATRES.201803042.

[10] L. Yin, Mingcai, Z.Z. Zhaosheng, Jiahui Kou, Mechanism investigation of visible light-induced degradation in a heterogeneous TiO_2/eosinY/Rhodamine B system, Environ Sci Technol 43 (2009) 8361–8366.

[11] L. Chen, J. Tang, L.-N. Song, P. Chen, J. He, C.T. Au, S.F. Yin, Heterogeneous photocatalysis for selective oxidation of alcohols and hydrocarbons, Appl Catal B Environ 242 (2019) 379–388, http://dx.doi.org/10.1016/J.APCATB.201810025.

[12] A. Mishra, A. Mehta, S. Basu, Clay supported TiO_2 nanoparticles for photocatalytic degradation of environmental pollutants: a review, J Environ Chem Eng 6 (2018) 6088–6107, http://dx.doi.org/10.1016/J.JECE.201809029.

[13] B. Szczepanik, Photocatalytic degradation of organic contaminants over clay-TiO_2 nanocomposites: a review, Appl Clay Sci 141 (2017) 227–239, http://dx.doi.org/10.1016/J.CLAY.201702029.

[14] E.M. Rangel, C.C.N. de Melo, F.M. Machado, Ceramic foam decorated with ZnO for photodegradation of Rhodamine B dye, Boletín La Soc Española Cerámica y Vidr 58 (2019) 134–140, http://dx.doi.org/10.1016/J.BSECV.201810002.

[15] P.C. Ricci, C.M. Carbonaro, L. Stagi, M. Salis, A. Casu, S. Enzo, F. Delogu, Anatase-to-rutile phase transition in TiO_2 nanoparticles irradiated by visible light, J Phys Chem C 117 (2013) 7850–7857, http://dx.doi.org/10.1021/jp312325h.

[16] H. You, Z. Wu, Y. Jia, X. Xu, Y. Xia, Z. Han, Y. Wang, High-efficiency and mechano-/photo-bi-catalysis of piezoelectric-ZnO@ photoelectric-TiO_2 core-shell nanofibers for dye decomposition, Chemosphere 183 (2017) 528–535, http://dx.doi.org/10.1016/J.CHEMOSPHERE.201705130.

[17] S. Javed, M. Islam, M. Mujahid, Synthesis and characterization of TiO_2 quantum dots by sol gel reflux condensation method, Ceram Int 45 (2019) 2676–2679, http://dx.doi.org/10.1016/J.CERAMINT.201810163.

[18] M.K. de Almeida, Ê.L. Machado, D.A.R. Lopez, P.A.M. dos Santos, C.P.A. de Bergmann, A.L. Rodriguez, Synthesis of TiO_2-based photocatalysts and their use in the degradation of the semi-precious-gemstone-coloring dye rhodamine B, FME Trans 46 (2018) 259–265, http://dx.doi.org/10.5937/fmet1802259K.

[19] P. Roy, S. Berger, P. Schmuki, TiO_2 nanotubes: synthesis and applications, Angew Chem Int Ed 50 (2011) 2904–2939, http://dx.doi.org/10.1002/anie.201001374.

[20] A. Najafi, F. Golestani-Fard, H.R. Rezaie, Sol-gel synthesis and characterization of B4C nanopowder, Ceram Int 44 (2018) 21386–21394, http://dx.doi.org/10.1016/J.CERAMINT.201808196.

[21] W.A. Thompson, C. Perier, M.M. Maroto-Valer, Systematic study of sol-gel parameters on TiO_2 coating for CO_2 photoreduction, Appl Catal B Environ 238 (2018) 136–146, http://dx.doi.org/10.1016/J.APCATB.201807018.

[22] A. Manassero, M.L. Satuf, O.M. Alfano, Photocatalytic reactors with suspended and immobilized TiO_2: comparative efficiency evaluation, Chem Eng J 326 (2017) 29–36, http://dx.doi.org/10.1016/J.CEJ.201705087.

[23] D. Chen, F. Li, A.K. Ray, External and internal mass transfer effect on photocatalytic degradation, 2001 https://ac.els-cdn.com/S0920586101002565/1-s2.0-S09205861 01002565-main.pdf?_tid=81b5b96d-2049-4e5c-a003-fe6c7cc2d 19c&acdnat=1542980764_6f44ef8af05097c2689ad79eeabbfb49 [accessed 23.11.18].

[24] R. Oblak, M. Kete, U.L. Štangar, M. Tasbihi, Alternative support materials for titania photocatalyst towards degradation of organic pollutants, J Water Process Eng 23 (2018) 142–150, http://dx.doi.org/10.1016/J.JWPE.201803015.

[25] M.C. Bordes, A. Moreno, E. Bou, V. Sanz, Cerámica y Vidrio sobre soporte cerámico, Cerámica y Vidr 46 (2007) 273–279.

[26] A.R.A.A. Scharnberg, V. Priebbnow, S. Arcaro, R.M. Da Silva, P.A.M. Dos Santos, T.M. Basegio, A.A.L. Rodriguez, Evaluation of the addition of soda-lime glass and yerba mate wastes in ceramic matrix, Cerâmica 65 (2019) 63–69 http://www.scielo.br/scielo.php?script=sci_arttext&pid=S0366-69132019000100063&lng=en&nrm=iso.

[27] R.F. De Mello Peters, P.A.M. Dos Santos, T.C. Machado, D.A.R. Lopez, Ê.L. Machado, A. De Assis Lawisch Rodriguez, Photocatalytic degradation of methylene blue using TiO_2 supported in ceramic material, Eclet Quim 43 (2018) 26–32, http://dx.doi.org/10.26850/1678-4618eqj.v43.1.26-32.

[28] G.S. Falk, M. Borlaf, M.J. López-Muñoz, J.B. Rodrigues Neto, R. Moreno, Photocatalytic activity of nanocrystalline $TiNb_2O_7$ obtained by a colloidal sol-gel route, Ceram Int 44 (2018) 7122–7127, http://dx.doi.org/10.1016/j.ceramint.2018.01.153.

[29] J.R. Lakowicz, Principles of frequency-domain fluorescence spectroscopy and applications to protein fluorescence, Cell Struct Funct Microspectrofluorom (1989) 163–184, http://dx.doi.org/10.1016/B978-0-12-417760-4.50016-1.

[30] C.H. Wu, J.M. Chern, Kinetics of photocatalytic decomposition of methylene blue, Ind Eng Chem Res 45 (2006) 6450–6457, http://dx.doi.org/10.1021/IE0602759.

[31] U. Balachandran, N.G. Eror, Raman spectra of titanium dioxide, J Solid State Chem 42 (1982) 276–282, http://dx.doi.org/10.1016/0022-4596(82)90006-8.

[32] S. Silvestri, M.G. Gonçalves, P.A. da Silva Veiga, T.T. da, S. Matos, P. Peralta-Zamora, A.S. Mangrich, TiO_2 supported on Salvinia molesta biochar for heterogeneous photocatalytic degradation of Acid Orange 7 dye, J Environ Chem Eng 7 (2019) 102879, http://dx.doi.org/10.1016/J.JECE.2019.102879.

[33] A.L. Linsebigler, G. Lu, J.T. Yates, Photocatalysis on TiO_2 surfaces: principles, mechanisms, and selected results, Chem Rev 95 (1995) 735–758, http://dx.doi.org/10.1021/cr00035a013.

[34] Z. Zhang, P.A. Maggard, Investigation of photocatalytically-active hydrated forms of amorphous titania, $TiO_2 \cdot nH_2O$, J Photochem Photobiol A: Chem 186 (2007) 8–13, http://dx.doi.org/10.1016/J.JPHOTOCHEM.200607004.

[35] S. Lebrette, C. Pagnoux, P. Abélard, Stability of aqueous TiO_2 suspensions: influence of ethanol, J Colloid Interface Sci 280 (2004) 400–408, http://dx.doi.org/10.1016/J.JCIS.200407033.

[36] T. Luttrell, S. Halpegamage, J. Tao, A. Kramer, E. Sutter, M. Batzill, Why is anatase a better photocatalyst than rutile? – model studies on epitaxial TiO_2 films, Sci Rep 4 (2015) 1–8, http://dx.doi.org/10.1038/srep04043.

[37] T.B. Wermuth, A.L. Rodriguez, C.P. Bergmann, A. Straatmann, Descolorimento de efluente associado ao tingimento de ágatas contendo Rodamina B com diferentes combinações fotocatalíticas via processos oxidativos avançados (POA's), Tecno-Lógica 17 (2013) 117–123, http://dx.doi.org/10.17058/TECNOLOG.V17I2.3984.

[38] A. Mishra, A. Mehta, M. Sharma, S. Basu, Enhanced heterogeneous photodegradation of VOC and dye using microwave synthesized TiO_2/Clay nanocomposites: a comparison study of different type of clays, J Alloys Compd 694 (2017) 574–580, http://dx.doi.org/10.1016/J.JALLCOM.201610036.